Supplement of The Cryosphere, 14, 4719–4733, 2020
https://doi.org/10.5194/tc-14-4719-2020-supplement

The Cryosphere
Open Access

Supplement of

Scoring Antarctic surface mass balance in climate models to refine future projections

Tessa Gorte et al.

Correspondence to: Tessa Gorte (tessa.gorte@colorado.edu)

1 Section S1

The top three modes of AIS SMB variability in the reconstruction are the only three modes with the percent of variance explained above 10% (Fig. S 1). In total, these top three modes explain about 77% of the total variance in AIS SMB in the reconstruction.

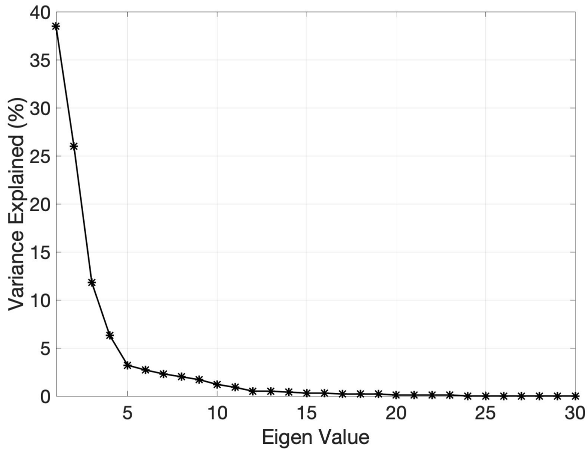

Figure S 1. The top 30 Eigen values out of 200 total for SMB in the reconstruction. The top three Eigenvalues explain 76.3% of the total SMB variance.

To gain insight into what atmospheric conditions may lead to the dominant modes of SMB spatial variability, we performed the same EOF analysis on the reconstructed sea level pressure (Fig. S 2). The top mode of atmospheric variability shows high variability around the Amundsen Sea region. Similarly, mode 2 also reflects strong variability in the Amundsen Sea region but with more zonal symmetry. The third mode of atmospheric variability represents a quadripolar pattern in variability about the 0-180° and 90°E/W longitude lines.

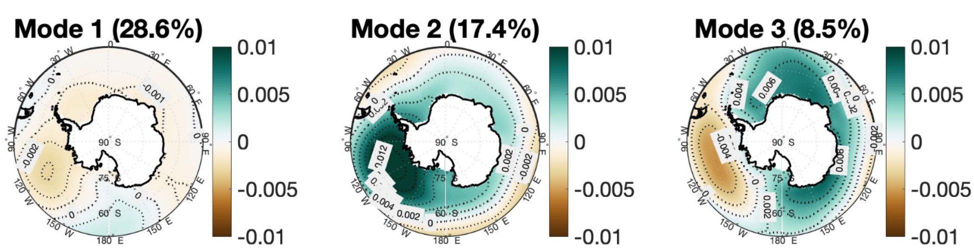

Figure S 2. EOFs of the top 3 modes of the reconstruction for sea level pressure.

2 Section S2

The average final score for CMIP5 is 3.7 and the average final score for CMIP5 is 5.6. To determine if this difference is generated by the smaller CMIP6 sample size, we performed a Monte Carlo-type simulation. Randomly selecting 22 of the 41 total CMIP5 model scores 10,000 times, we then tested whether those 10,000 selections were statistically different from all 41 using a two-sided t-test. The t-test generates results of 0 if we cannot reject the null hypothesis that the two samples are different at the 95% confidence level or 1 if we can. Averaging the t-test over all 10,000 selections yields a 0.042% chance that we can reject the null hypothesis. From this, we determine that we cannot reasonably reject the null hypothesis that these two scores are statistically different at the 95% confidence level. This means that 22 models is representative of the total CMIP5 suite of models from which we hypothesize that the same can be said for the current 22 models being representative of the full CMIP6 suite of models in terms of average final score.

3 Section S3

To assess how much of the model sensitivity to forcing scenario is attributable to spread in ΔT versus spread in $\frac{\Delta \mathrm{SMB}}{\Delta \mathrm{T}}$, we compared the relative spreads of each. For RCPs 2.6, 4.5, and 8.5, respectively, $\frac{\Delta \mathrm{SMB}}{\Delta \mathrm{T}}$ ranged between -116% to + 305%, 21% to 264%, and 52% to 223% about their respective means. By comparison, ΔT ranged between 56% to 156%, 30% to 141%, and 45% to 135% about their relative means for RCPs 2.6, 4.5, and 8.5, respectively. In short, ΔT ranged about 100% about the mean in each scenario while $\frac{\Delta \mathrm{SMB}}{\Delta \mathrm{T}}$ ranged about 200% to 300% about the mean depending on scenario. With that, we conclude that much of the variation in $\frac{\Delta \mathrm{SMB}}{\Delta \mathrm{T}}$ between models stems from differences in how the models react to different forcing scenarios rather than owing to large spread in modeled temperature change over the 21st century.

4 Section S4

Internal variability – the process by which model ensemble members deviate due to small changes in model initialization – potentially plays a large role in overall model score. Figure 4 shows the scores of the 5 CESM members that appear in the CMIP5 suite as well as 35 ensemble members from the CESM-LENS experiment. The spread in CESM-LENS is comparable to that of the CMIP5 CESM simulations. This spread is largely generated by variability in the EOF criteria. From the sizeable spread, we conclude that internal variability can potentially be as significant as specific parameterization choices within a single model. The spread in CESM-LENS is significantly smaller, though, than the spread across all CMIP5 models indicating that model physics are the dominant factor in the reproduction of AIS SMB.

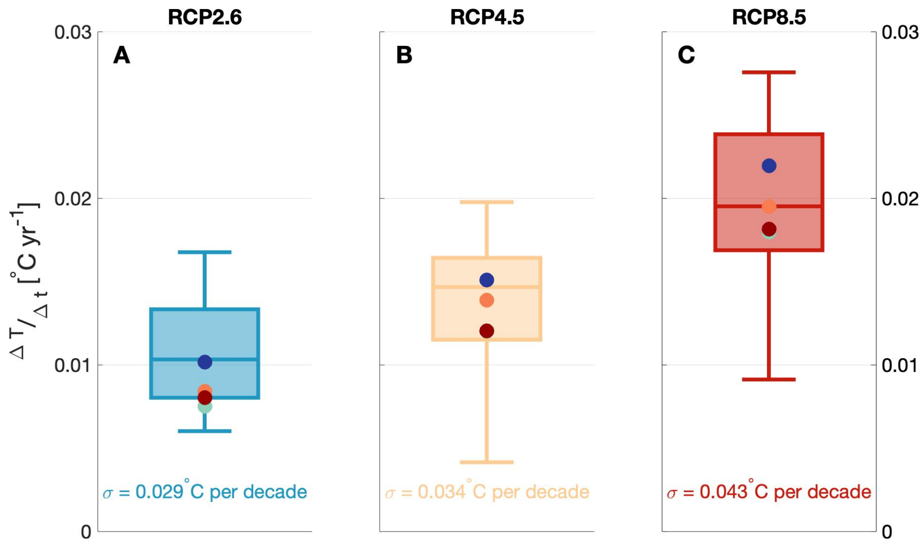

Figure S 3. Box plots of the temperature trends in $^{\circ}$C yr^{-1} for **A** RCP2.6 (blue), **B** RCP4.5 (yellow), and **C** RCP8.5 (red). The four best scoring models are shown as colored circles: GISS E2 H (dark blue), GISS E2 R (green), MPI ESM LR (coral), and MPI ESM MR (dark red).

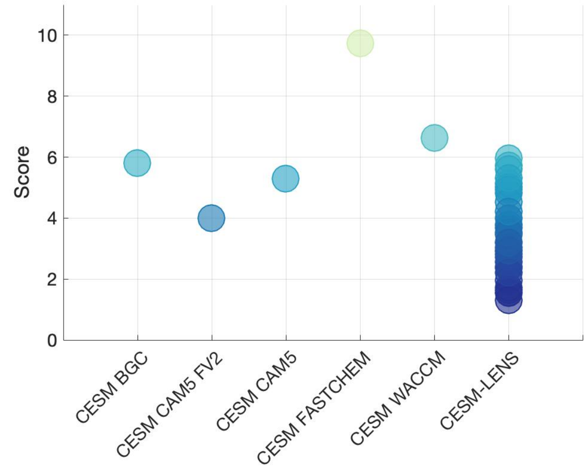

Figure S 4. Final scores of the five CESM models from CMIP5 compared to the CEMS-LENS simulations.

4.1 Subsection S4.1

We calculated the reconstruction uncertainty used in the AIS-integrated criteria as

$$totaluncertainty = \sqrt{(reconstructionuncertainty)^2 + (internalvariabilityuncertainty)^2}. \tag{1}$$

Through our analysis of the CESM LENS experiment, we generated the internal variability as one standard deviation of the raw values of AIS-integrated, temporally averaged mean value, AIS-integrated trend, and AIS-integrated variability (Fig. S 3). With this internal variability, we then calculated the reconstructed uncertainty used throughout the paper. The difference between the observational uncertainty and the reconstruction uncertainty for the three AIS-integrated criteria is small which aligns with our analysis that the EOF criteria generated the largest spread in score among the CESM LENS ensemble members.

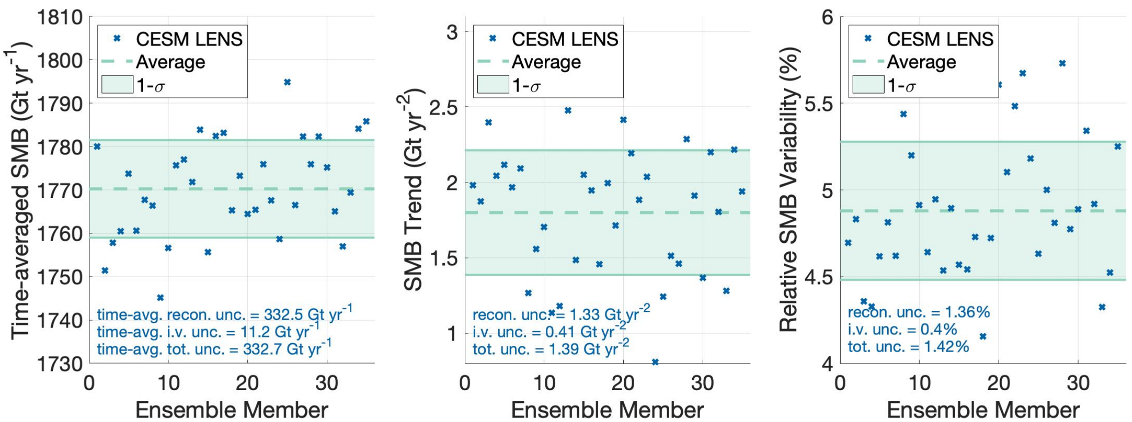

Figure S 5. Scatter plots of CESM LENS ensemble member and their AIS-integrated, temporally averaged mean value **A**, AIS-integrated trend **B**, and AIS-integrated variability **C**. The dashed green line shows the ensemble average and the green shaded box denotes one standard deviation (1-σ).

5 Section S5

To investigate the importance of model resolution for overall model score, we perform a linear regression analysis. Figure 6 shows all model resolutions plotted against their overall scores. Here, regression analysis shows a statistically significant, albeit relatively small, correlation coefficient of -0.4 with 95% confidence intervals of -0.62 and -0.17.

6 Section S6

Of the eight best scoring models, seven originate from two modeling centers: the Max Planck Institute fr Meteorologie (MPI) and Goddard Institute for Space Studies (GISS) from NASA. This strongly implies that model physics plays a significant role

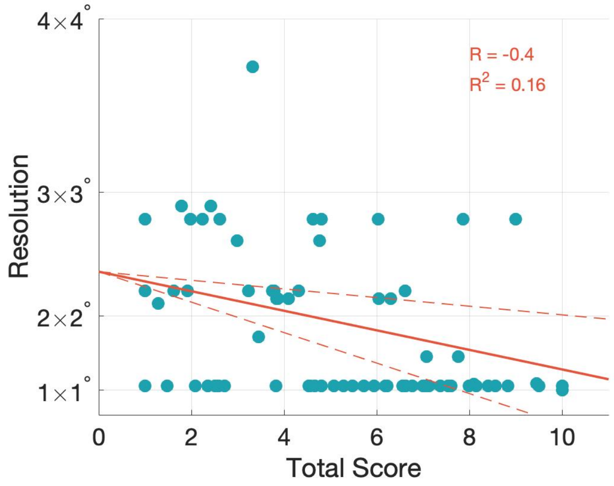

Figure S 6. Scatter plot of resolution versus total score. A linear regression (orange line) yields a correlation of R = 0.45 with 95% confidence intervals (orange dashed lines) of 0.30 and 0.61.

in the representation of AIS SMB. Another interpretation could be, though, that these models simply share the same biases and, thus, all are coincidentally favorably compared to the reconstruction. Here, we also look at a more diverse spread of modeling centers in two ways: 1) the top eight models that originate from unique modeling centers and 2) the top four modeling centers (top 90th percentile) averaged across their members. Figures S 7 and S 8 show the best scoring eight models from unique modeling centers and best four scoring modeling centers on average, respectively. The former category consists of GISS R, MPI ESM LR, CESM2 FV2, FGOALS G2, MIROC ESM, INM CM4, IPSL CM5A MR, and ACCESS ESM1-5 (Fig. S 7). MPI ESM, GISS, FGOALS, and INM CM from CMIP5 constitute the latter category of best modeling centers on average (Fig. S 8).

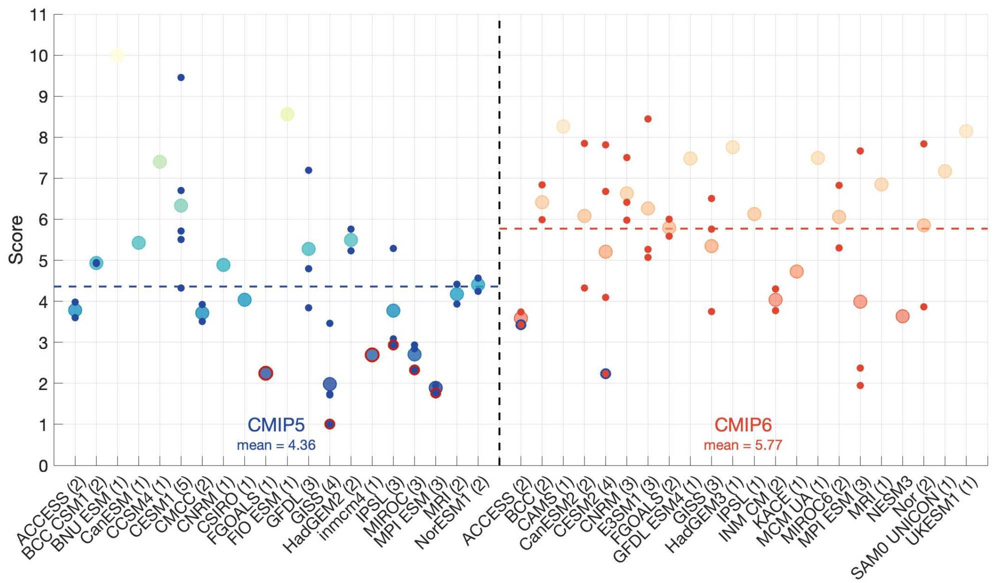

Figure S 7. The scores for all CMIP5 and CMIP6 models. The large dots show the average score for all model groupings. Models are grouped by similar model physics and have in parentheses the number of models in the grouping after the name. Each model grouping has all model scores plotted as small blue/red dots for CMIP5/6 with the model average plotted in the larger dots. Models that have no like models are followed by a one in parentheses and only have a larger dot. Unlike Figure 7 in the Results section of the main text, this figure highlights the eight best scoring models from unique modeling centers (i.e. no one modeling center can have more than one of the top eight models) which are denoted with red outlines if they are among the CMIP5 suite of models or with blue outlines if they are among the CMIP6 suite of models. The eight best modeling centers, then, are GISS, MPI, FGOALS, MIROC, INM, and IPSL from CMIP5 and CESM2 and ACCESS from CMIP6.

7 Section S7

This section includes tables with model resolutions and scores for all CMIP5 and CMIP6 models as well as a table with projected SMB and related variables for the various RCPs.

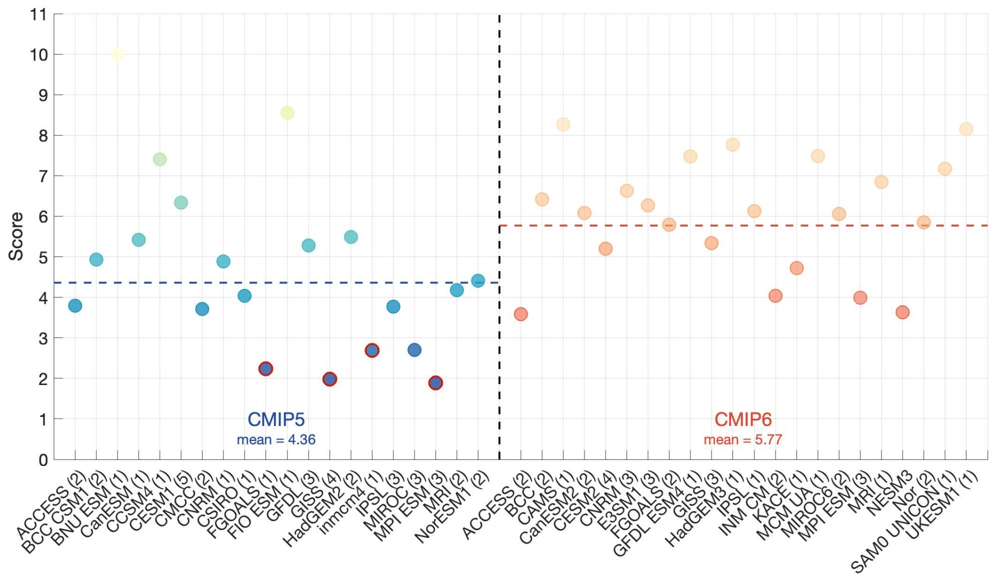

Figure S 8. The scores for all CMIP5 and CMIP6 models. The dots show the average score for all model groupings. Models are grouped by similar model physics and have in parentheses the number of models in the grouping after the name. Here, the top scoring 4 modeling centers (90th percentile of 41 modeling centers) on average are denoted with red outlines as they are all within the CMIP5 suite of models. The four best modeling centers on average are MPI, GISS, FGOALS, MIROC, and INM from CMIP5.

	Model	Resolution (°lat×°lon)	Total Score
1	ACCESS1-0	1.2414×1.875	3.80
2	ACCESS1-3	1.2414×1.875	3.38
3	BCC-CSM1.1	2.8125×2.8125	4.85
4	BCC-CSM1.1-m	2.8125×2.8125	4.99
5	BNU ESM	2.8125×2.8125	10
6	CanESM2	2.8125×2.8125	5.24
7	CCSM4	0.9375×1.25	7.40
8	CESM1 BGC	0.9375×1.25	5.81
9	CESM1 CAM5 FV2	0.9375×1.25	3.99
10	CESM1 CAM5	0.9375×1.25	5.30
11	CESM1 FASTCHEM	0.9375×1.25	9.74
12	CESM1 WACCM	0.9375×1.25	6.63

Table S 1. Model names, resolutions and final score for the first half of the CMIP5 suite of models.

	Model	Resolution (°lat×°lon)	Total Score
13	CMCC CESM	0.75×0.75	3.94
14	CMCC CM	0.75×0.75	3.50
15	CNRM CM5	1.4063×1.4063	4.73
16	CSIRO	1.875×1.875	3.98
17	FGOALS	3×2.8125	2.07
18	FIO ESM	2.8125×2.8125	8.89
19	GFDL CM3	2×2.5	3.83
20	GFDL ESM2G	2×2.5	4.48
21	GFDL ESM2M	2×2.5	7.11
22	GISS E2 H CC	2×2.5	1.72
23	GISS E2 H	2×2.5	3.55
24	GISS E2 R CC	2×2.5	1.60
25	GISS E2 R	2×2.5	1.00
26	HadGEM2 CC	1.2414×1.875	5.14
27	HadGEM2 ES	1.2414×1.875	5.56
28	INMCM4	1.5×2	2.61
29	IPSL CM5A LR	1.875×3.75	3.13
30	IPSL CM5A MR	1.2587×2.5	2.88
31	IPSL CM5B LR	1.875×3.75	5.50
32	MIROC ESM CHEM	1.4063×1.4063	2.75
33	MIROC ESM	2.8125×2.8125	2.86
34	MIROC5	2.8125×2.8125	2.19
35	MPI ESM LR	1.875×1.875	1.59
36	MPI ESM MR	1.067×1.067	1.76
37	MPI ESM P	1.875×1.875	1.76
38	MRI CGCM3	1.125×1.125	3.92
39	MRI ESM1	1.125×1.125	4.46
40	NorESM1 M	1.875×2.5	3.89
41	NorESM1 ME	1.875×2.5	4.30

Table S 2. Model names, resolutions and final score for the second half of the CMIP5 suite of models.

	Model	Resolution ($^{\circ}$lat$\times$$^{\circ}$lon)	Total Score
1	ACCESS CM2	1.25×1.875	3.66
2	ACCESS ESM1-5	1.25×1.875	3.25
3	BCC CSM2 MR	1.125×1.125	7.17
4	BCC ESM1	2.8125×2.8125	6.20
5	CAMS CSM1	1.125×1.125	8.78
6	CanESM5	2.8125×2.8125	8.25
7	CanESM5-CanOE	2.8125×2.8125	4.42
8	CESM2	0.9375×1.25	8.04
9	CESM2 FV2	1.9×2.5	2.08
10	CESM2 WACCM	0.9375×1.25	6.93
11	CESM2 WACCM FV2	1.9×2.5	3.76
12	CNRM CM6-1	1.4063×1.4063	6.63
13	CNRM CM6-1-HR	0.5×0.5	8.10
14	CNRM ESM2	1.4063×1.4063	6.09
15	E3SM1	1.0×1.0	8.79
16	E3SM1-1	1.0×1.0	5.17
17	E3SM1-1 ECA	1.0×1.0	5.09
18	FGOALS F3 L	2.0×2.25	5.88
19	FGOALS G3	2.0×2.25	5.72
20	GFDL ESM4	1.0×1.25	7.71
21	GISS E2 G	2.0×2.5	5.81
22	GISS E2 G CC	2.0×2.5	3.55
23	GISS E2 H	2.0×2.5	6.78
24	HadGEM3 GC3	1.25×1.875	7.97
25	IPSL CM6A	1.2587×2.5	6.30
26	INM CM4-8	1.5×2.0	3.66
27	INM CM5-0	1.5×2.0	4.04
28	KACE1-0-G	1.25×1.875	4.78
29	MCM UA1	2.25×3.75	8.42
30	MIROC6	2.8125×2.8125	7.14
31	MIROC E2SL	2.8125×2.8125	5.38

Table S 3. Model names, resolutions and final score for the first half of CMIP6 suite of models.

	Model	Resolution (°lat×°lon)	Total Score
32	MPI ESM1-2-HAM	1.875×1.875	2.16
33	MPI ESM1-2-HR	0.935×0.935	8.04
34	MPI ESM1-2-LR	1.875×1.875	1.77
35	MRI ESM2	1.125×1.125	7.16
36	NESM3	1.875×1.875	3.45
37	NorCPM1	1.875×2.5	8.00
38	NorESM2-MM	0.9375×1.25	3.80
39	SAM0 UNICON	0.9375×1.25	7.58
40	UKESM1	0.9375×1.875	8.45

Table S 4. Model names, resolutions and final score for the second half of CMIP6 suite of models.

8 Section S8

Figure 9 shows the AIS with the names of locations specifically mentioned in the main text.

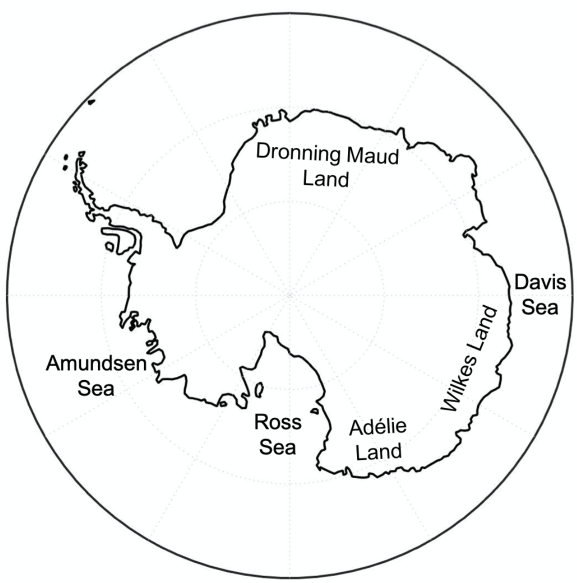

Figure S 9. Map of the AIS.